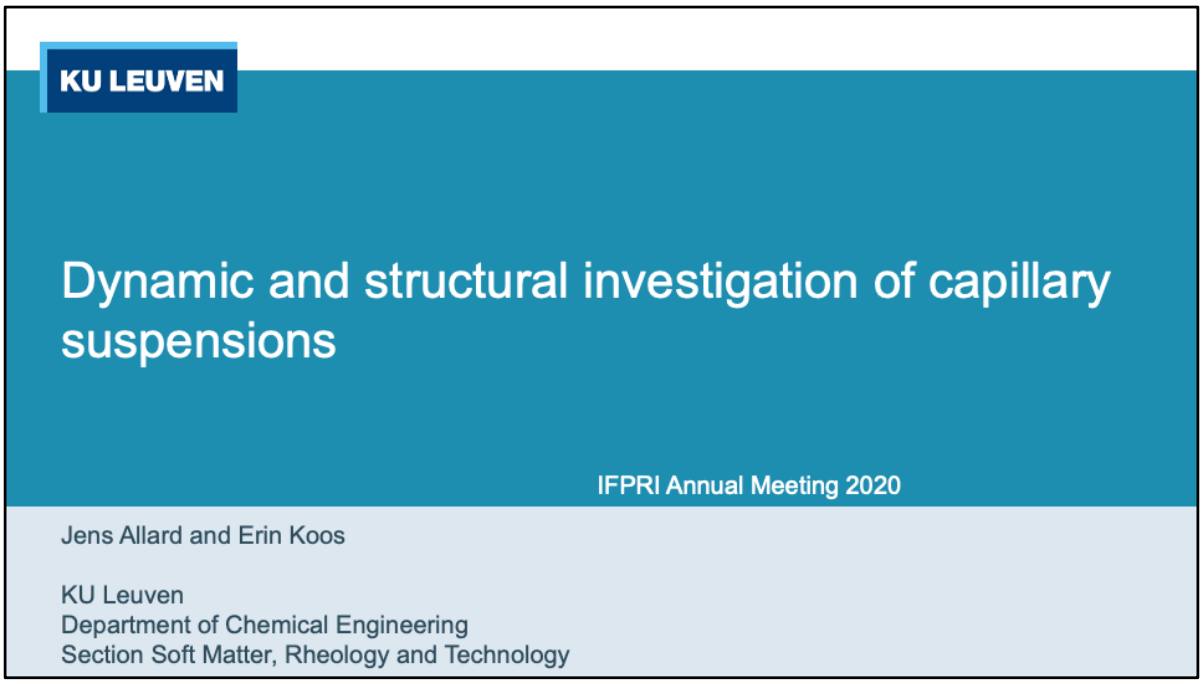

Hello and thank you for listening to (reading) this online version of our presentation at the IFPRI Annual Meeting 2020.

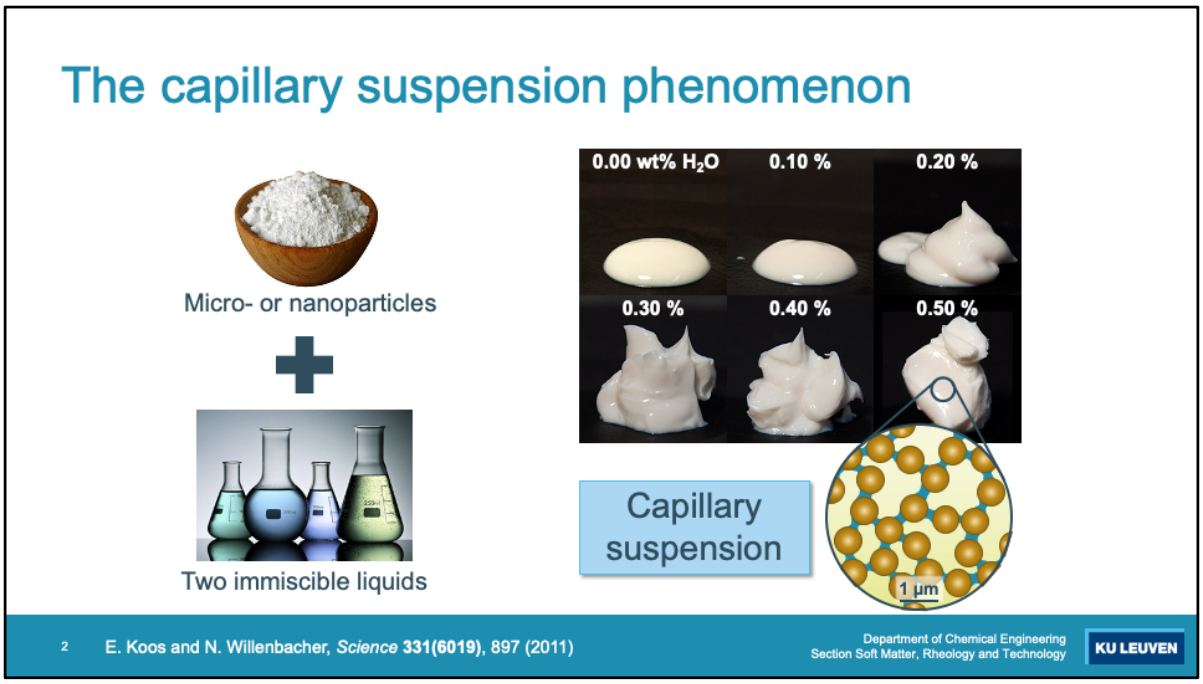

To start, let us quickly remind you about capillary suspensions. Capillary suspensions are solid-liquid-liquid systems, typically formed when a small amount of a secondary liquid is added to a suspension of micro- or nanoparticles. The two liquids must be (partial) immiscible and the secondary fluid is often present in only a few percent. This secondary liquid leads to the formation of a sample-spanning particle network caused by the capillary attraction between the particles. This is like the addition of small amounts of water to the grains of sand in a sandcastle, but here our grains are much smaller, the air is replaced by a liquid, and we usually have a much lower particle loading.

As can be seen in the example on the right, a dramatic change in the bulk properties of the materials occurs with very small amounts of liquid. In this case, using a suspension of calcium carbonate in an oil with small amounts of water, less than 0.5% water by weight increases the yield stress and viscosity by several orders of magnitude.

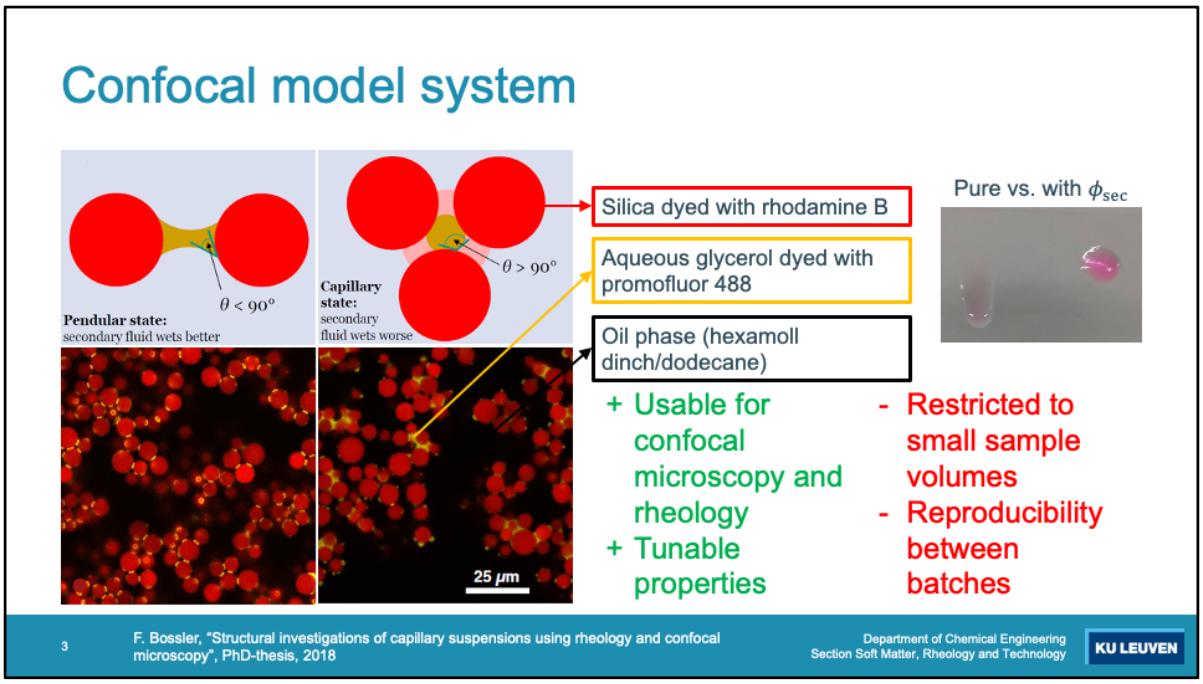

To investigate the structure of these networks, we use a confocal model system composed of silica particles dyed with rhodamine B isothiocyanate. These particles (at least in this part of the project) are porous and the dye is covalently bonded to both the particle interior and exterior. The aqueous phase, which is usually the secondary phase in these experiments, is a mixture of water and glycerol dyed with promofluor 488. In the confocal images on the left, the particles are shown in red and the secondary fluid in yellow. The oil phase is undyed and appears black on the images. Without secondary liquid, the pure suspension freely flows (upper right image) whereas it shows gel-like properties with a volume of added secondary liquid ϕ_{sec}. By using silica particles, we can change the three-phase contact angle θ through silanization. This lets us switch between the pendular state $\theta < 90°$ where the secondary liquid preferentially wets the particles, forming binary bridges between the particles, and the capillary state $\theta > 90°$ where the particles from small clusters surrounding the secondary liquid droplets.

This index-matched system is applicable to both confocal microscopy and can also be used for simple rheological measurements. We have carefully controlled the mixing procedure to ensure that the samples are uniform. Thus, the structure should be identical throughout the sample volume and we won't make mistakes by inferring changes in the material structure when it's only an error caused by the sampling location. Furthermore, we can tune the sample properties: the ratio of the three components and the contact angle.

…

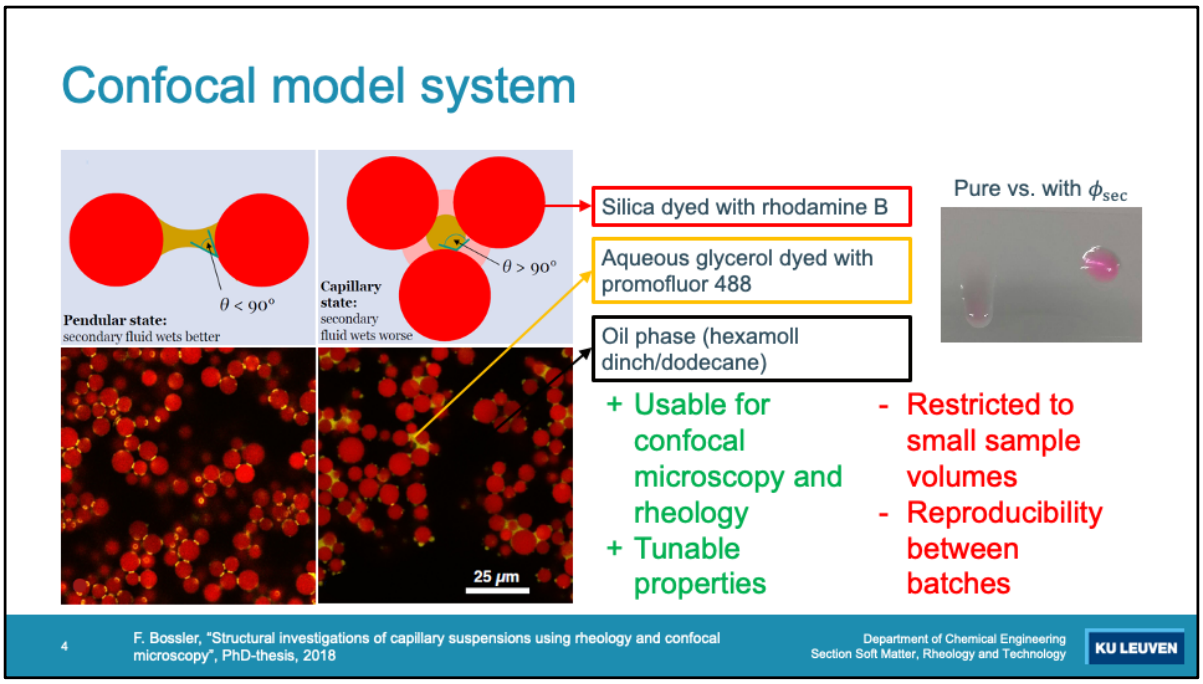

This isn't the perfect model system, however. The mixing procedure used to create uniform samples restricts us to sample sizes less than 1 ml. This means we can make rheological measurements using a small plate-plate geometry, but not a Couette cell or vane. The silanization process also lacks in reproducibility; the exact same processing steps and amounts can result in a change in the contact angle by more than 10º. Therefore, experiment runs are limited by the batch size.

Despite these drawbacks, this is still the best system we have been able to use to study the connection between rheology and structure.

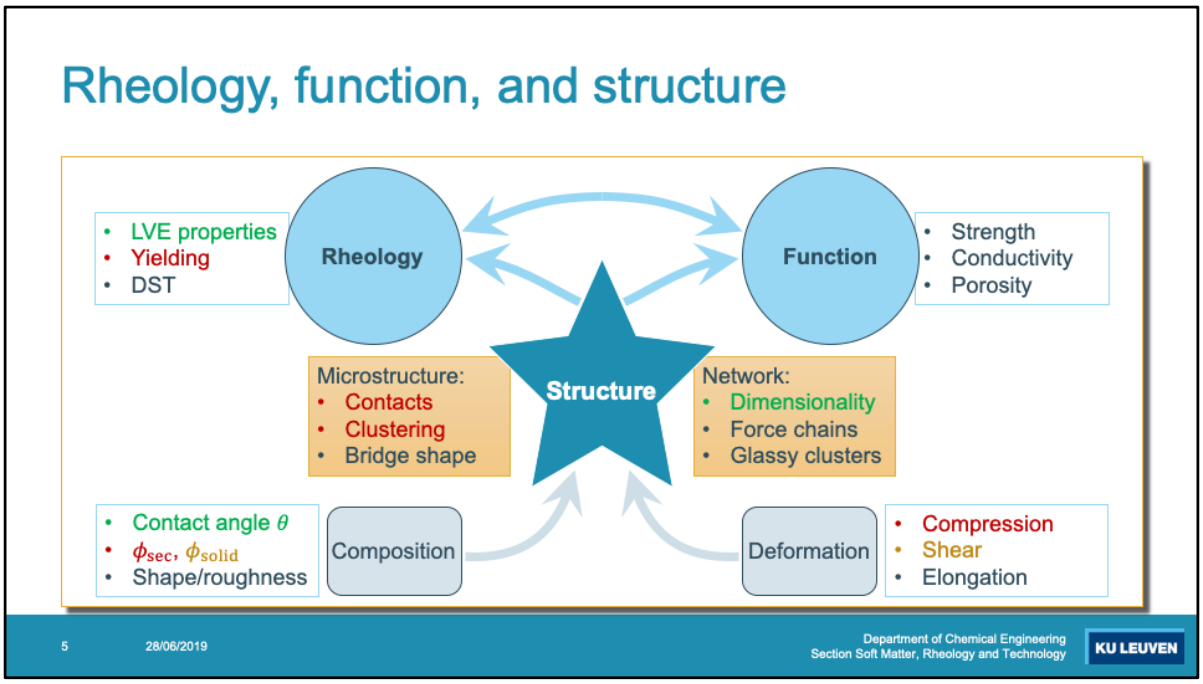

The goal of this project is to connect rheology (for example, the properties in the linear viscoelastic region, yielding, and shear thickening) and function (e.g. strength, conductivity porosity) through the structure of these samples. This structure depends on the sample composition and external deformation. If we can understand these relations, we can predict the behavior and design better materials. Typically, we think about structure at two extreme length scales: the microstructure at the size of the particles and the network structure at length scales much larger than the particle size. In this project, we also want to determine which length scale is important and to find rigorous measures that work at many different length scales.

We started this process previously, looking at the influence of the solid loading ϕ_{solid} and contact angle θ on the linear viscoelastic LVE properties and using this to design new materials. These properties were connected to the material structure through the network dimensionality. This year, we have concentrated on the influence of the secondary fluid content ϕ_{sec} using microstructural measures such as the number of contacts and clustering coefficient. We also investigated the influence of compression and shear on the material properties at different solid loadings.

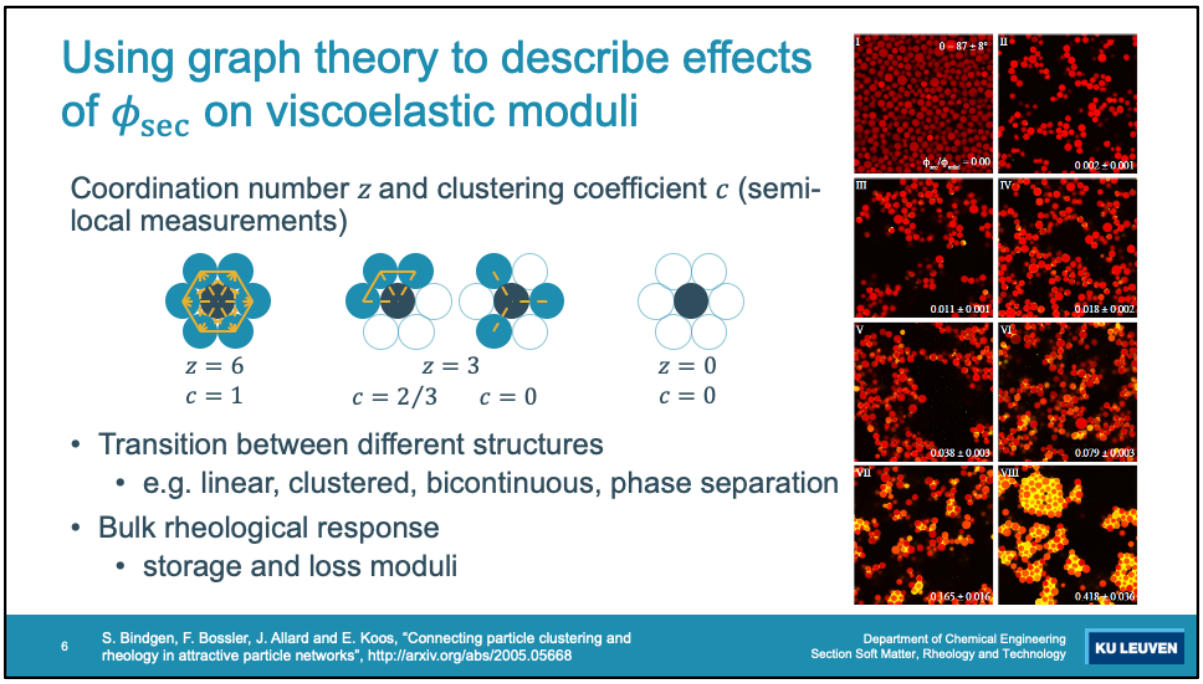

If we take, for instance, the influence of the secondary fluid volume fraction, you can see a wide variety of different structures that can be created. Without added liquid, there is no interaction between the particles and a granular pile forms. At point II, were only a small amount of aqueous glycerol is added, you can see a dramatic change in the structure. Even though there are no clear bridges shown here – they are much smaller than the size of the particles – the attractive force is sufficient to prevent particle sedimentation. As the amount of secondary liquid is increased, these bridges grow and merge to create small clusters. At point VII, you can clearly see these bridges connecting multiple particles. While there is undoubtedly a sample-spanning network in this sample, the clusters are still isolated from each other with binary bridges in between. This is termed the funicular state. At point VIII, the particle-secondary fluid clusters become fully connected and a bicontinuous structure is formed. Finally, the sample will phase separate into a single dense cluster if more secondary liquid is added.

Since network-level measures such as the dimensionality are clearly insufficient to describe each and every ϕ_{sec} point in this sample, we must use a different measure. The number of neighbors, the coordination number z, which can be readily calculated from confocal images, provides some insights, but has a tenuous link to rheology. We therefore propose supplementing this measure with another measure from graph theory, namely the clustering coefficient, as shown in the sketch.

…

Using graph theory to describe effects of ϕ_{sec} on viscoelastic moduli

Coordination number z and clustering coefficient c (semi-local measurements)

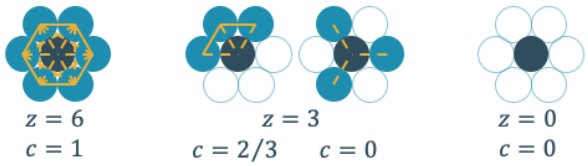

- Transition between different structures
  - e.g. linear, clustered, bicontinuous, phase separation
- Bulk rheological response
  - storage and loss moduli

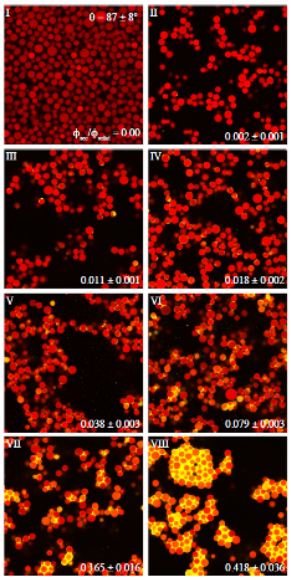

7 S. Bindgen, F. Bossler, J. Allard and E. Koos, "Connecting particle clustering and rheology in attractive particle networks", http://arxiv.org/abs/2005.05668

Department of Chemical Engineering
Section Soft Matter, Rheology and Technology
KU LEUVEN

The local clustering coefficient is defined as

$$c = \frac{2e}{z(z-1)},$$

where the number of bonds between neighbors (dashed lines) is z and the connections between these neighbors (solid lines) is e. An alternative definition of the clustering coefficient can be achieved by counting the number of triangles through a node (particle) compared to the number of neighbors

As illustrated in the sketch intermediate coordination numbers can either have low clustering ($c \to 0$) or high clustering ($c \to 1$) with clear implications of the mechanical response of the cluster. Although the upper limit of the clustering coefficient is $c = 1$, as shown in the non-physical packed structure on the left, real, e.g., biological networks, almost never reach this limit and $c > 0.5$ is considered as high clustering.

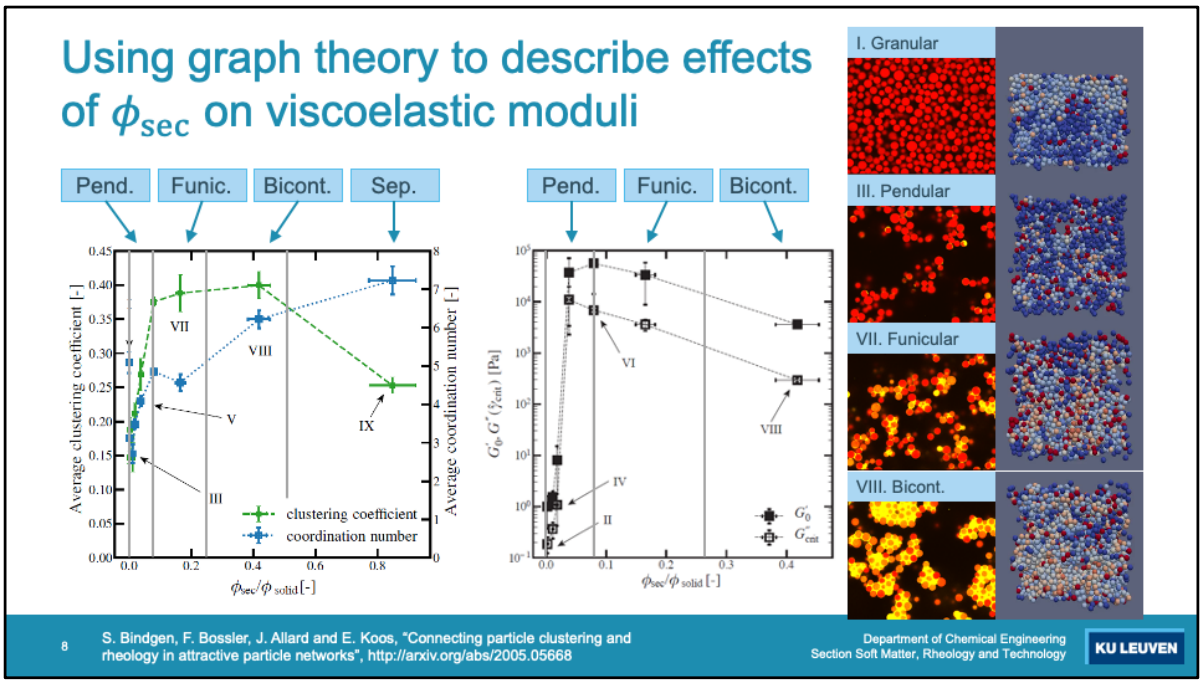

In a paper we recently placed on arXiv (and submitted to a journal for review), we used these measures to compare samples at two different contact angles, one in the pendular state and one in the capillary state. Changes in both the average $\bar{z}$ and $\bar{c}$ as well as in their distribution (captured here for a few key samples in the videos showing the networks where the particles are colored by their local clustering coefficient) can be quantified and correlated to rheological measurements. While the average values give some indication for the changes in the network structure, key transitions can be hidden by subtle changes in the average values.

A broad distribution of coordination numbers can be seen for the sample without added secondary liquid (top) with a mean value of $\bar{z} = 5.1$. The mean value of the clustering coefficient is $\bar{c} = 0.15$. A lot of particles with a clustering coefficient around the theoretical minimum of $c = 0$ can be observed, indicating particles without tight clustering. These values are characteristic for a loosely packed sedimented bed. That means there is a random arrangement of particles present where polydispersity of the particles can lead to a lot of isolated particles or particles with only one neighbor. This low clustering can indicate a metastable structure. Indeed, the structure of this sample changed slightly during the measurements, either due to the small movements of the objective or very slow sedimentation.

…

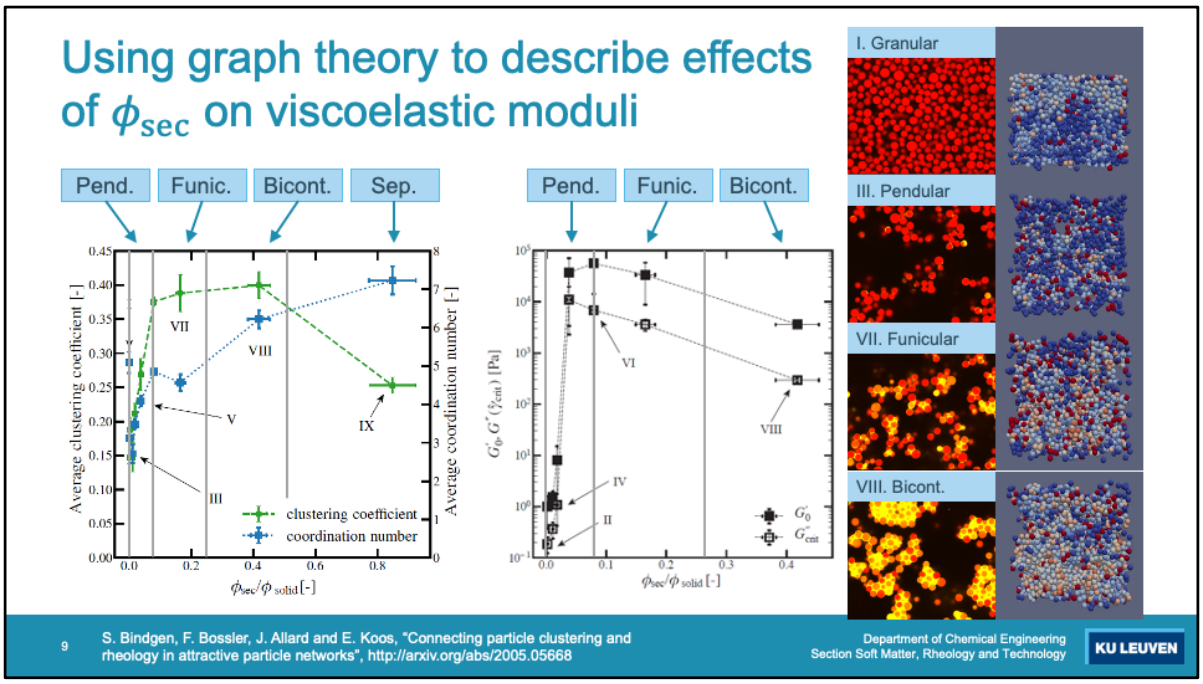

With the addition of secondary fluid to point III, we can see the structural arrangements due to the filling of the particle asperities. Particles are connected to each other via binary bridges leading to a lower average contact number of $\bar{z} = 2.7$ while the average clustering coefficient rises to $\bar{c} = 0.15$. This rise is caused by an increase in the number of particles with intermediate ($c = 0.3$) and high ($c = 1$) clustering. This is consistent with particles in a partially reinforced backbone chain. We conclude from the corresponding histogram that there is a change from the random sediment arrangement into an open network with many short, linear branches of two or three. Indeed, the amount of particles with a coordination number of $z = 2$ reaches its global maximum compared with the other histograms at point III. These values are consistent with the formation of a weak gel structure dominated by binary contacts and some tightly arranged clusters formed by trimers or other low number particle groups.

As the structure changes towards a funicular, or clustered, state (point IV), the coordination number increases. The average clustering coefficient also increases, but this change in the average is quite modest. The histogram shows a clearer loss in the number of particles with very low clustering and an increase in the intermediate clustering. This change is caused by the addition of particles to already existing clusters, leading to their increase in size and not by the formation of entirely new groups of particles.

…

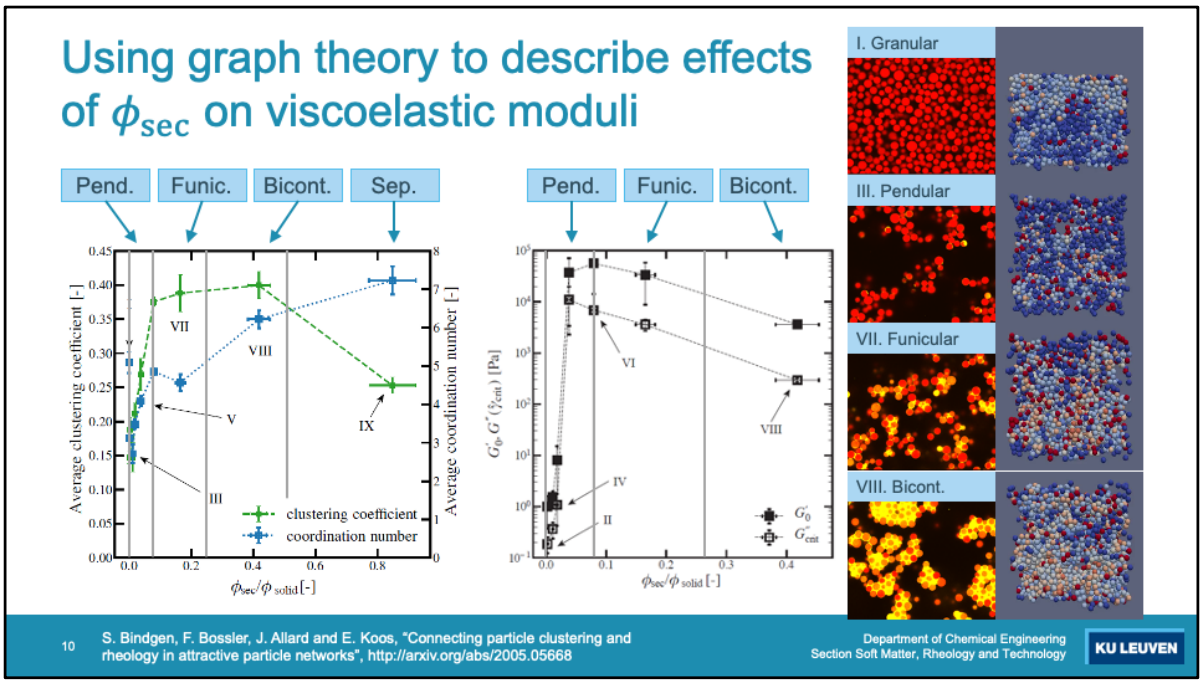

As the structure changes towards a funicular, or clustered, state (point IV), the coordination number increases. The average clustering coefficient also increases, but this change in the average is quite modest. The histogram shows a clearer loss in the number of particles with very low clustering and an increase in the intermediate clustering. This change is caused by the growth of clusters rather than the formation of entirely new groups of particles.

For the bicontinuous structure (point VII), the average coordination number has a value of $\bar{z} = 4.6$ while the clustering coefficient approaches a plateau with average values $\bar{c} = 0.39$. These are values that are typical of small-world phenomena in graph theory. Small world graphs have nodes that are not direct neighbors (low z or degree) but are only separated from each other by a few hops (a few particles). Put another way, these graphs are composed of tight cliques with few connections between cliques. A look at the confocal images reveals the presence of particle groups that become more and more isolated.

With the final addition of secondary fluid, the structure phase separates. This is indicated by the clustering coefficient decreasing towards the initial sedimented bed state. However, the structure seems to be denser than the initial sediment, as shown by the increased clustering coefficient and coordination number. This can be explained by the fact that the secondary liquid is solely present between the sedimented particles, pulling them together more tightly. This means that the arrangement of particles is not as random as in the first state without secondary liquid added. This structure should be more resilient to external deformation.

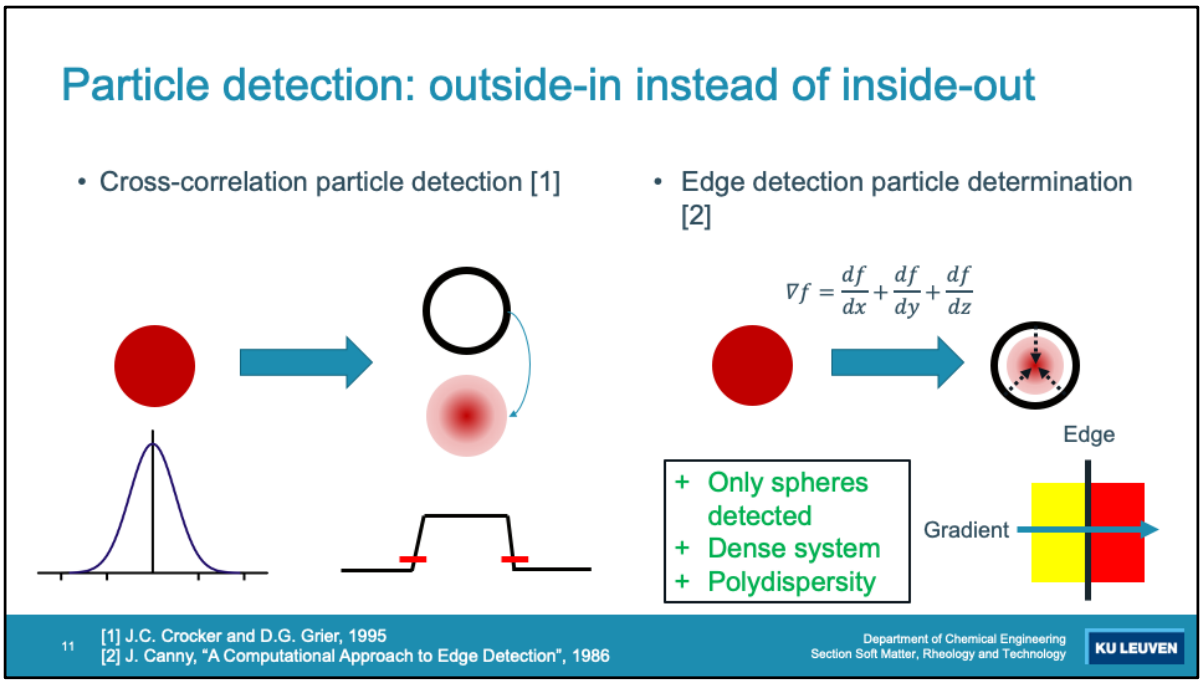

Moving on to the particle detection part, we see on the left a schematic of our previous approach based on the most widely-used particle detection program of Crocker and Grier. The image is convoluted with a Gaussian blur filter, which ideally transforms a particle in a bright center. These bright centers are detected in the next step with a cross-correlation mask. The radius is then determined by using a minimum cut-off intensity. The detection efficiency is very sensitive towards the size chosen for the Gaussian blur and the detection mask. Especially for a concentrated, polydisperse system, accidents are bound to happen: detecting two particles as one, or the other way around.

This is why the edge detection approach on the right was chosen. At the edge of the particle, a jump in intensity occurs. Thus, taking the image gradient, leaves us with these particle edges. For spheres, we have a huge advantage, in the sense that all gradients will point towards the center of the sphere. Next we vary the radius and let the edge pixels cast a vote in the direction of their gradient. The particle centers will be the pixels with the largest number of votes and will appear as bright centers. This process is called Hough transform (pronounced like tough). These bright centers can again be detected using the Crocker and Grier algorithm. Knowing the center and edge pixels, we can perform a least-squares fit of a sphere to determine the radius. For polydisperse samples, this approach is substantially more accurate.

To give you an illustration of how the edge detection works, Jens added a picture of himself (on the right). In this picture, the grass, for example, is bright so it has a high pixel value, while the darker shadows and the black dog have a low pixel value. Calculating the image gradient reveals the edges, which are the starting point for the detection. By the way, a lot of things are possible at this point. For example, you could try to extract from the right image the location of the laptop by looking for straight lines using the Hough transform. You can imagine though that in 3D, the computational cost of finding such specific shapes increases drastically.

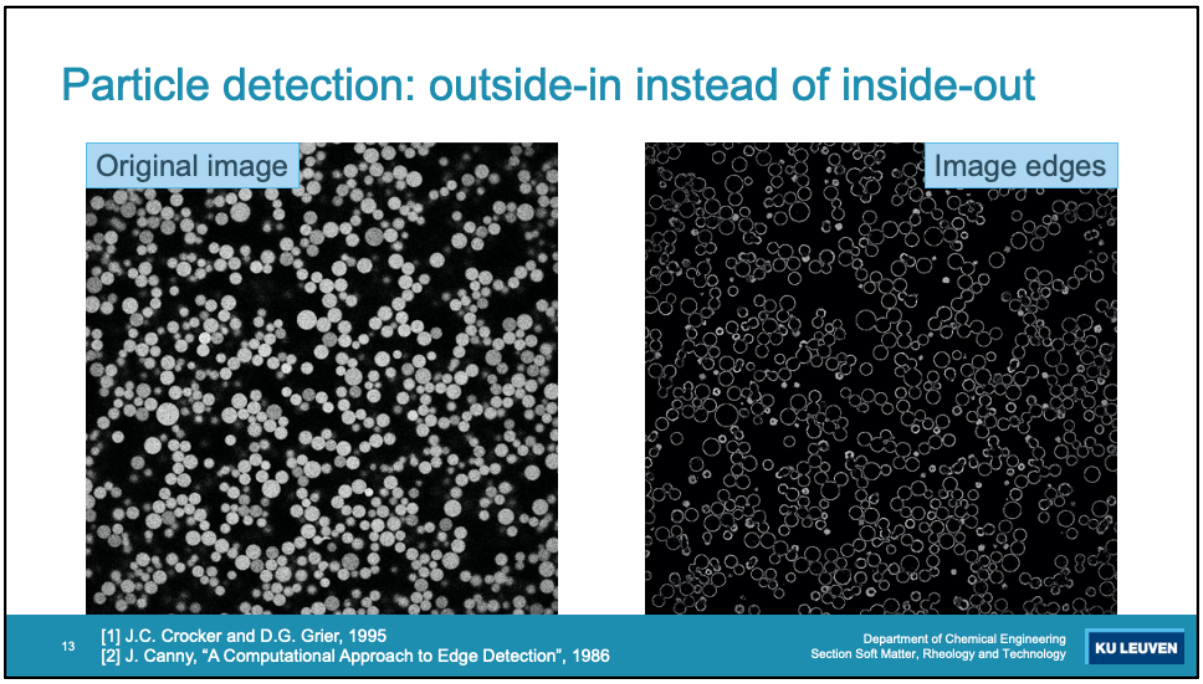

Luckily, as I mentioned before, the spherical particles greatly simplify the Hough transform step. All the pixels that remain on the right image point towards the center of their respective particle. By using a varying radius, we can find particle centers for this polydisperse, dense system.

Maybe I should make a short clarification for those of you wondering about the 3D detection. This is one 2D slice of the 3D image, which consists of taking 2D images at different heights in the sample. The particles which are not in focus on the left image, will be in focus on another slice. For the particle detection, this means their gradients point towards 2D slices above or below this one.

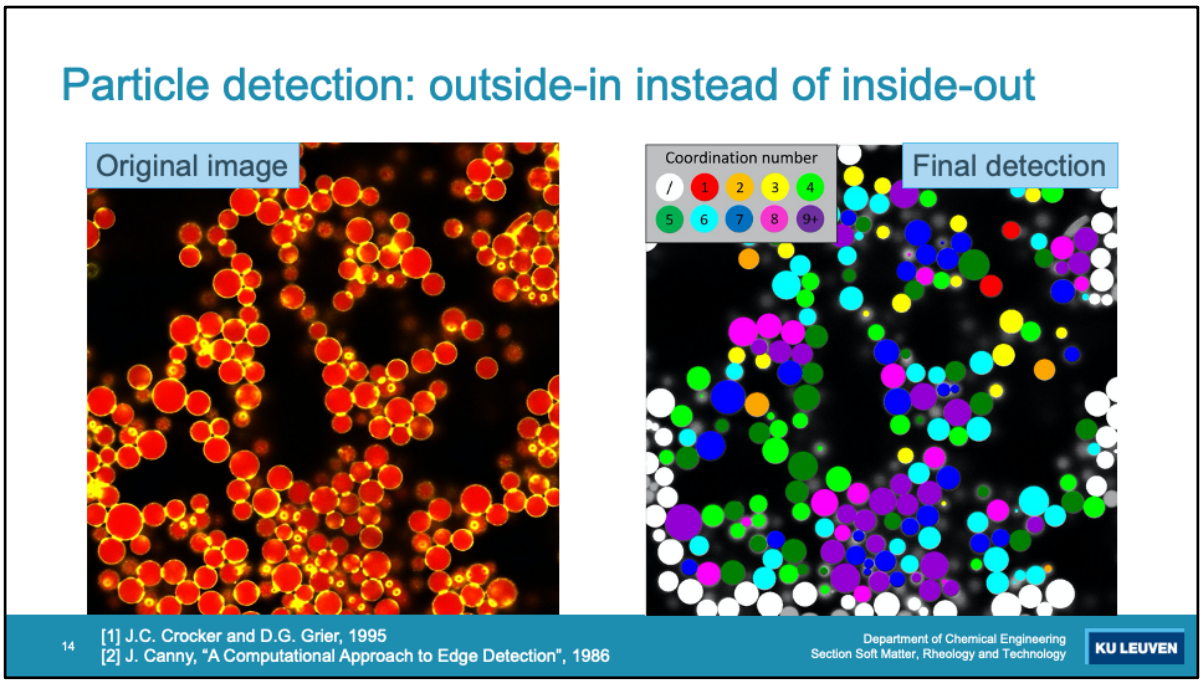

So to summarize, we start from a confocal image consisting of two colour channels: a yellow secondary fluid channel, which we don't really use for detection at this point, and a red particle channel. Using the edge detection and Hough transform we determine particle positions and radii. Once these are known, we can analyze the network using graph theory, for example with the coordination number. The image on the right shows particles with a low coordination number in red and orange, while high coordination numbers are shown in blue and purple. Particles at the edges are marked white, since we can't know their real coordination number. We considered two particles in contact, if their mutual distance falls below a threshold value. In reality, neighbouring particle connected by a bridge are in contact, but due to the resolution of the microscope and the accuracy of the detection, we chose the threshold equal to 6 pixels (0.85 µm).

A valuable upgrade to this code, would be to detect the bridge size and shape using the secondary fluid channel. This way, we can give a weight to each bond which will respresent the bond strength. When bonds start breaking under shear, we can quantify if the bond breaks due to low strength or its position in the network.

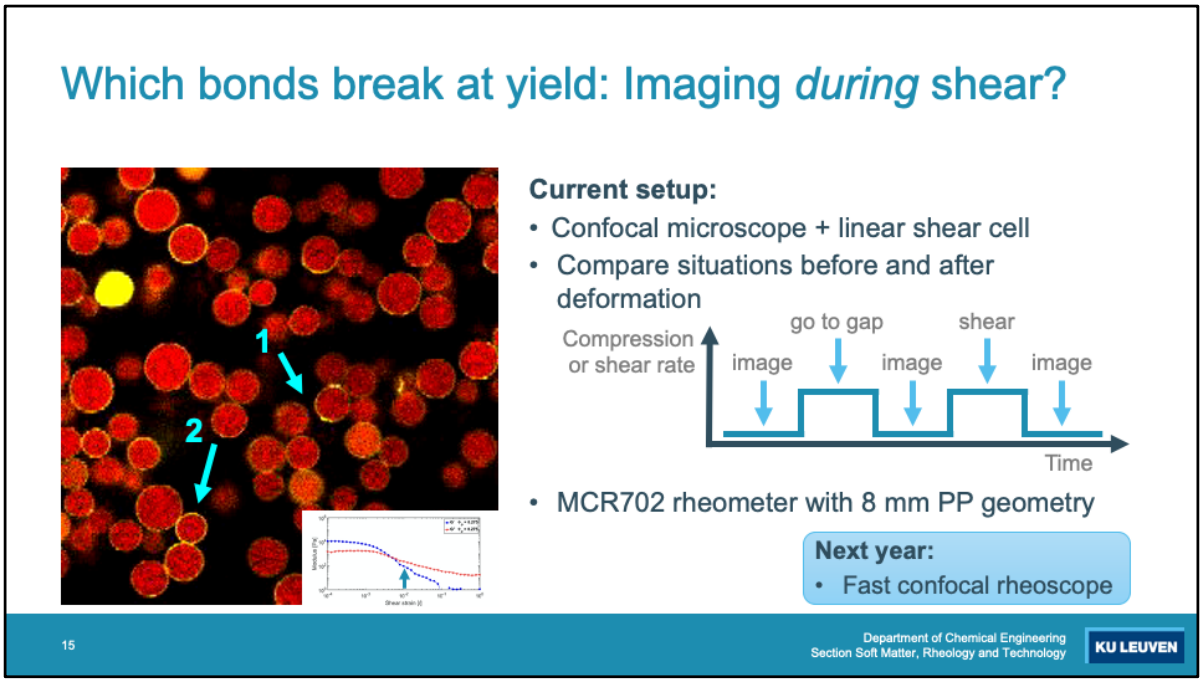

In this project, we want to go beyond the static measurements to investigate how the structure changes in response to external shear. In the video on the left, you can see the particle network deform and rearrange. There are two separate re-arrangement events. In 1, the particle attaches with its neighbor at about 6 seconds. In 2, the bond between these particles breaks at about 9 seconds. It's interesting to note that this video is taken just above the material flow point (crossover between G' and G''). If the material flows at this point, why do we only see two small events? Is this because most of the deformation happens in another location or are these two events critical in breaking the network structure?

To answer this question, we need to image the full network in 3D, ideally taking large images encompassing many particles. In our current setup, we have a linear shear cell attached to the confocal. The linear shear cell uses two microscope plates to deform the sample linearly, meaning that deformation is uniform regardless of the local x- and y-position. However, the speed of the confocal limits the size and deformation we can measure without distorting the image. To overcome this limitation, we have chosen to alternate between deforming and imaging. Since there is a sample-spanning network preventing particle motion in the absence of shear, we do not expect this periodic deformation profile to greatly affect the sample. Further, if the deformation is small, we can track the motion of the individual particles. Since the linear shear cell uses piezoelectric actuators, we cannot obtain stress measurements during deformation, so we must supplement this data with measurements on the rheometer.

Next year, we plan to attach a rheometer to our fast (sheet) confocal to take simultaneous deformation and stress measurements.

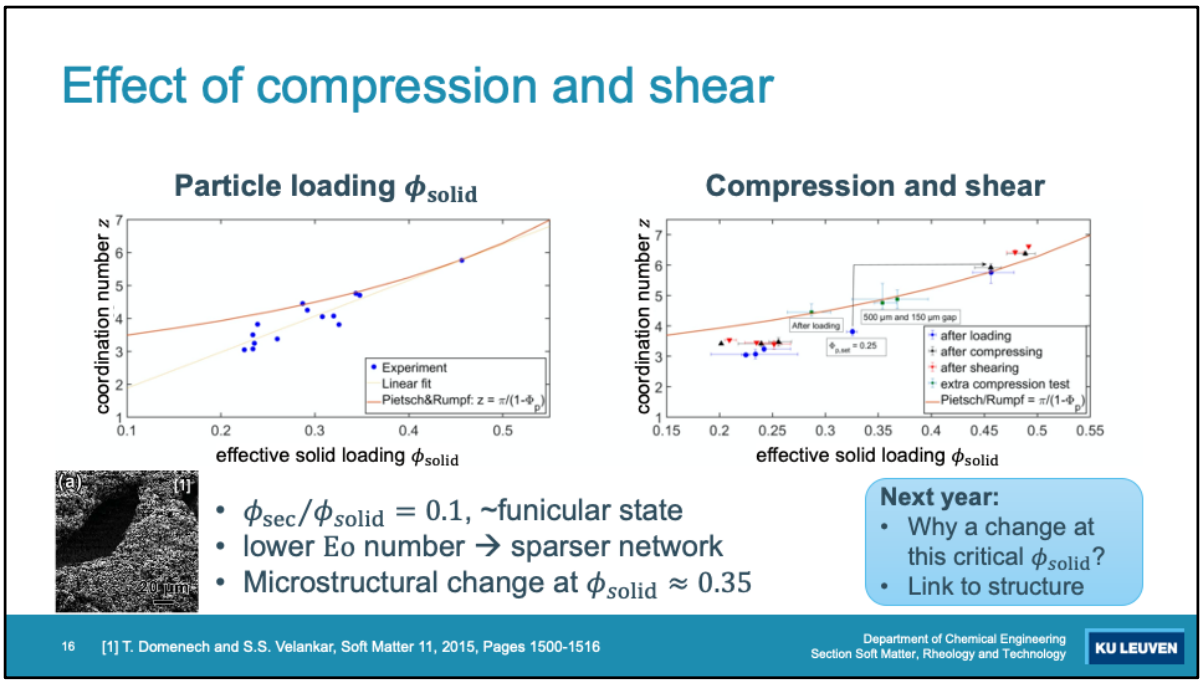

With our existing setup, we can still obtain a lot of information about the sample. Here, we show the effect of both particle loading and subsequent compression and shear on the coordination number z.

The coordination number obtained for different effective particle loadings is shown on the left for at $\phi_{sec}/\phi_{solid} = 0.1$ (near the funicular transition). The coordination number fits the trend proposed by Pietsch & Rumpf, $z = \pi/(1-\phi_{solid})$, at high loading. At lower solids, the coordination number deviates from this granular prediction and is shown with a linear fit. The Eötvös (or Bond) number, the ratio of capillary to gravitational forces, is typically smaller than unity ($\mathrm{Eo} \approx 0.01$ to 0.1) in granular matter but is much larger than for capillary suspensions ($\mathrm{Eo} \approx 10^{-5}$ to 10^{-6}). This produces sparser network in capillary suspensions. When the particle loading is high, however, the total weight of the clusters overcomes the capillary force to produce denser packings with more neighbors. The transition between the capillary-like and granular-like systems occurs at a volume fraction around $\phi_{solid} \approx 0.35$. This matches the results of Domenech and Velankar who observed large, capillary clusters (image) at $\phi_{solid} = 0.4$.

With compression and then shearing, the coordination number increases slightly, but there is no shift in the effective volume fraction ϕ_{solid} denoting compaction of the network for the sparse networks. At an initial volume fraction of $\phi_{solid,set} = 0.25$, however, the solid fraction increases dramatically to a value $\phi_{solid} = 0.46$. The even higher set volume fraction of $\phi_{solid,set} = 0.46$ also increases during the compression step. While these two points exhibit a strong resistance (high normal force) during the compression, they still compact more than the capillary-like samples. The shift in these

higher volume fraction samples follows the prediction of Pietsch and Rumpf.

…

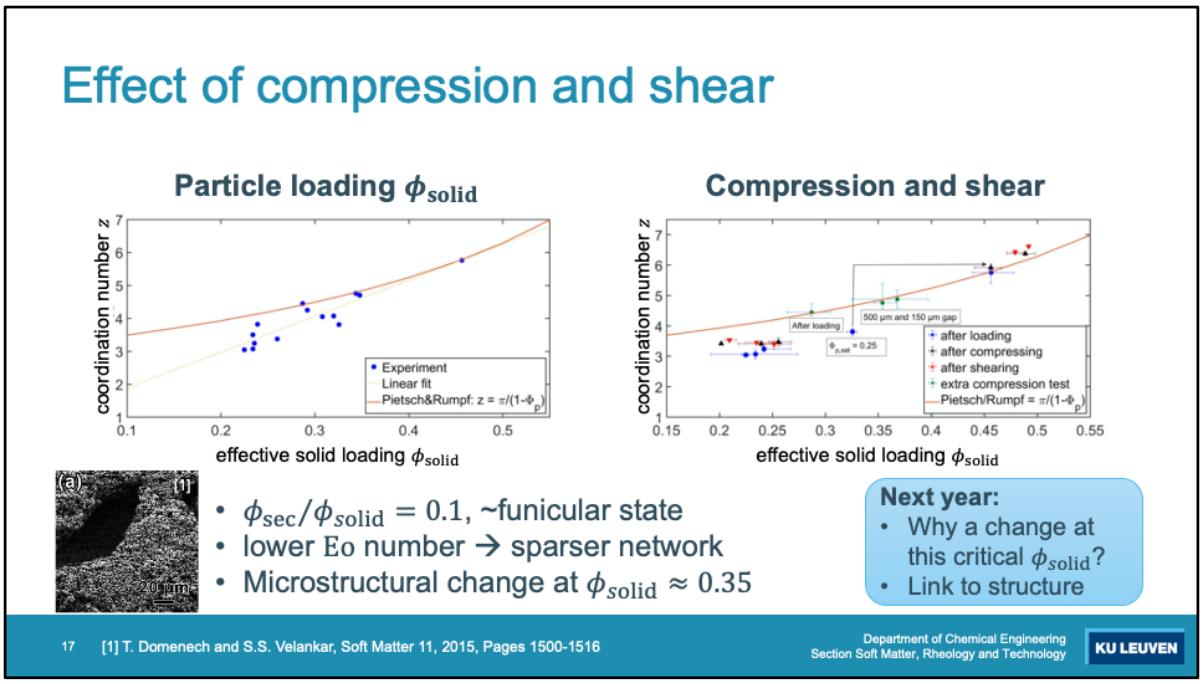

Interestingly, we conducted an extra experiment at a slightly lower set volume fraction of $\phi_{\mathrm{solid,set}} = 0.3$. Unlike the previous experiment, the initial coordination number is higher, fitting to the granular prediction. This increases with compression to a gap of 500 µm and then subsequent compression to a gap of 150 µm, but the change is less pronounced than the previous transitional sample.

To understand the differences between the capillary-like and granular-like systems and to understand why at transition is observed at this critical ϕ_{solid}, we will continue these experiments this next year. We want to make a clear link with the structure and want to understand why two networks, both in the transitional region, behaved so differently.

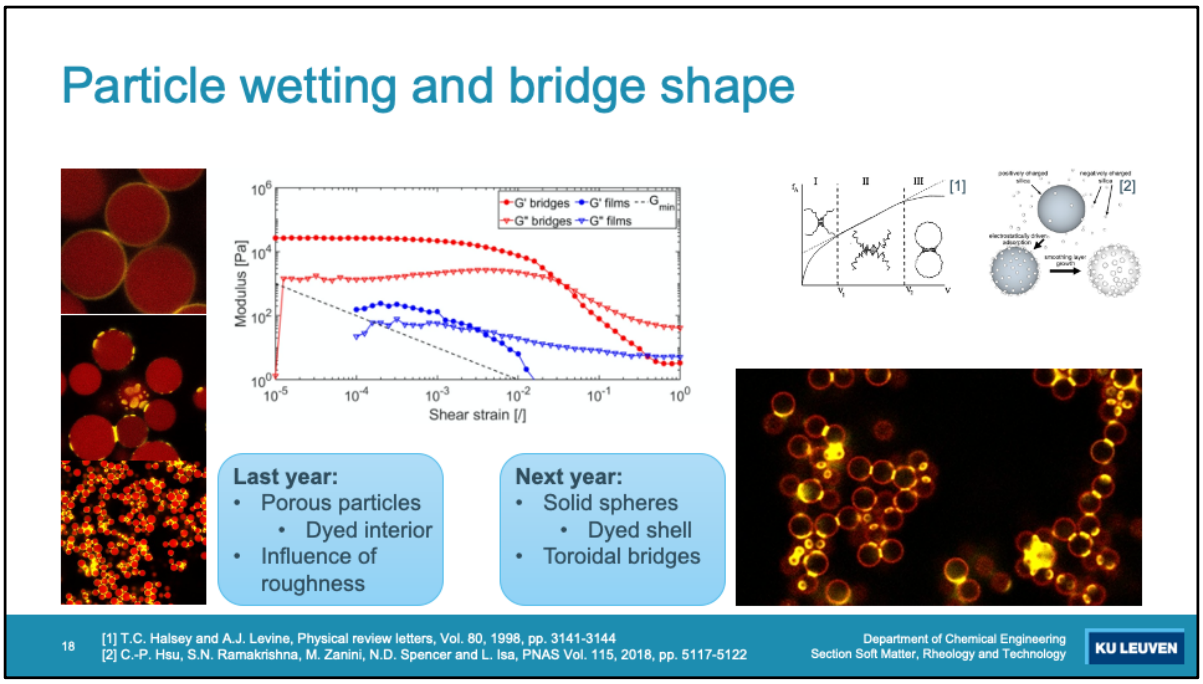

All the experiments performed so far, started from the same porous particles. After dyeing the particles, these pores are partially sealed off with a modified Stöber reaction to prevent, usually, the secondary fluid from being absorbed into the particles. However, as you see on the left, this resulted in different wetting behaviors which we assume to be caused by the surface roughness that remains after the pore closing reaction. At the top, we have a batch where only the surface asperities are wetted, forming a liquid film around the particles, without capillary bridges visible in the micrographs. In the middle, we see some sort of liquid patches on the particle surface, but not the toroidal or cylindrical bridge shape we ideally expect. The bottom image shows a funicular sample which did have toroidal bridges. Consistently, getting toroidal bridges proved to be difficult, due to the irreproducibility of the particle processing steps.

The rheological data shows the huge difference in moduli between proper bridges and films. The red data is obtained by making the same particles used for the blue data slightly more hydrophobic. Theoretically, a higher contact angle should correspond to a decrease in strength. However, this made it so the particles changed their wetting behavior from films to bridges, increasing both moduli by 2 orders of magnitude. The flow point is shifted to the right, since the liquid bridges are able to stretch before breaking, while this is much lesser the case for the film particles. The coordination number data shown earlier, was mostly obtained with film wetted particles.

…

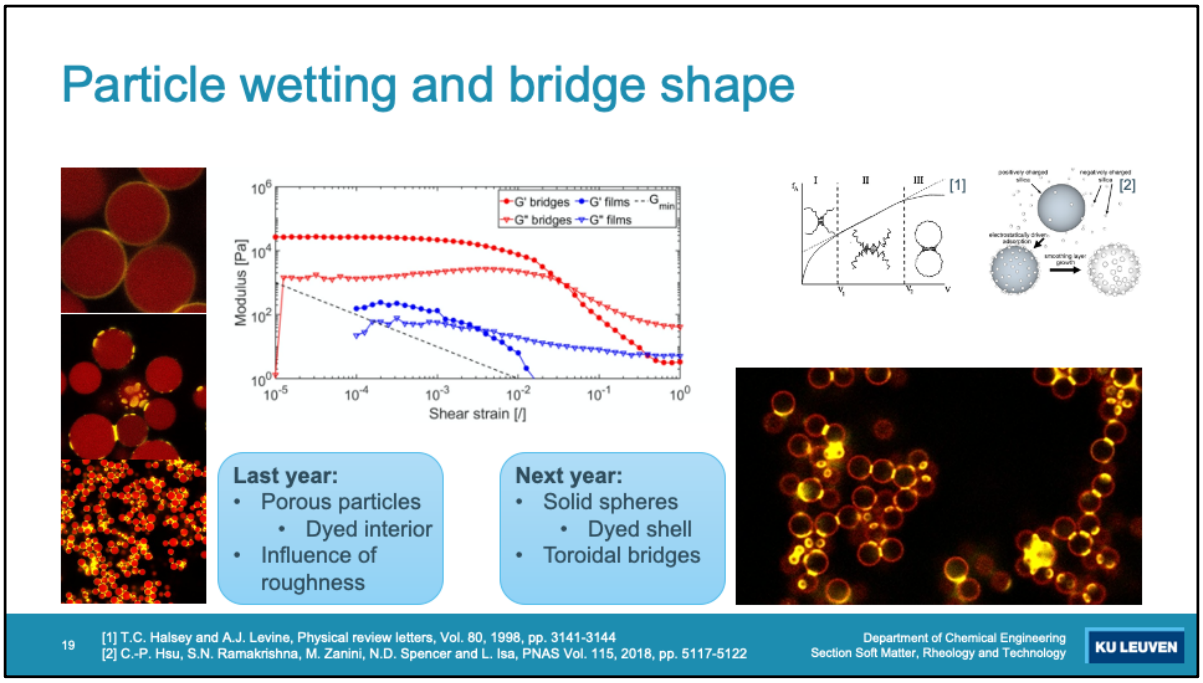

The possibly crucial influence of surface roughness will be investigated in detail next year by a Master thesis student. In this project, silica nanospheres will be adsorbed onto a micron-sized particle to create raspberry-like particles with varying roughness. We can hopefully recreate the three wetting behaviors on the left purposely, and identify the transitions from asperity wetting, to roughness wetting and finally toroidal bridges for which the surface roughness does not matter anymore compared to the curvature of the particle.

An obvious way to avoid the roughness problem is to switch to non-porous particles with a dyed shell. A batch of these was recently bought, and a confocal micrograph is shown on the bottom right picture. As you can see, the interior of the particles is no longer dyed. If we recall the two main particle detection methods, the cross-correlation Crocker/Grier algorithm would not be able to detect these particles. On the other hand, with edge detection and Hough transform, this becomes possible, but might introduce some difficulties which are shown on the next slide. These particles should however always show the same wetting behavior.

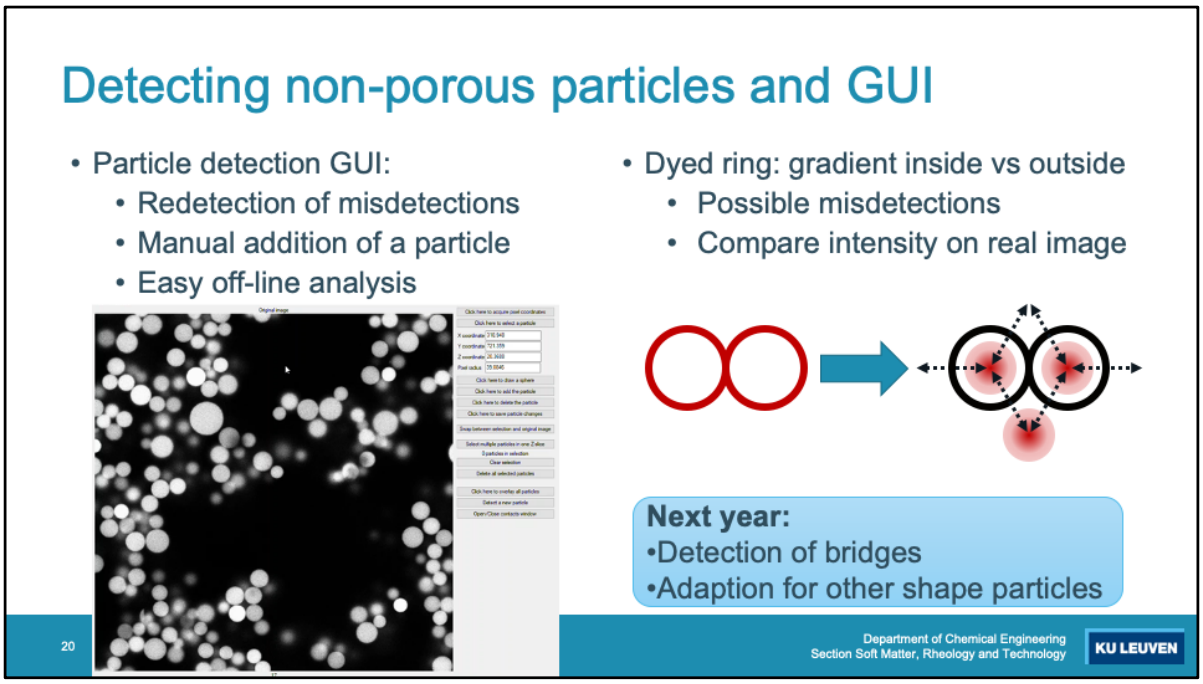

During the laboratory shutdown, we have had a chance to improve the particle detection. First, we have improved the detection of particles. These misdetections occur when small particles are detected as a single larger particle or larger particles are split into multiple smaller particles. One of the ways we have improved this detection is by implementing a GUI (shown in the video) where we can select particles, either redetecting their radii and centers, or manually select an approximate particle center and size to improve the detection. This GUI also lets us easily analyze the networks offline and better visualize the connections between particles so that we can understand the changes in the networks and link these changes to an applied deformation.

The switch to particles with a dyed ring, while it will undoubtedly be better to control the structure, presents some challenges in the detection of the particles. With the fully dyed particles, there is a clear gradient between the inside and the outside of the particles. This may result in possible misdetections where the gradient vector – which can now point both ways – can lead to phantom particle being detected near the intersection of two particles. To prevent this error, we can compare the intensity differences in the real images, looking for specific shaped (e.g. round) particles and use the secondary fluid channel to further give information about the inside or outside of the particle.

Next year, we will expand this detection algorithm to detect the size and shape of the bridges, a task that is again easier when we use the nonporous particles since the particle volume does not need to be “subtracted” from the bridges. We can also adapt the algorithm to adapt particles of different shapes. This detection should be more straightforward than the cross-correlation method since we will not have to use masks

with many different orientations.

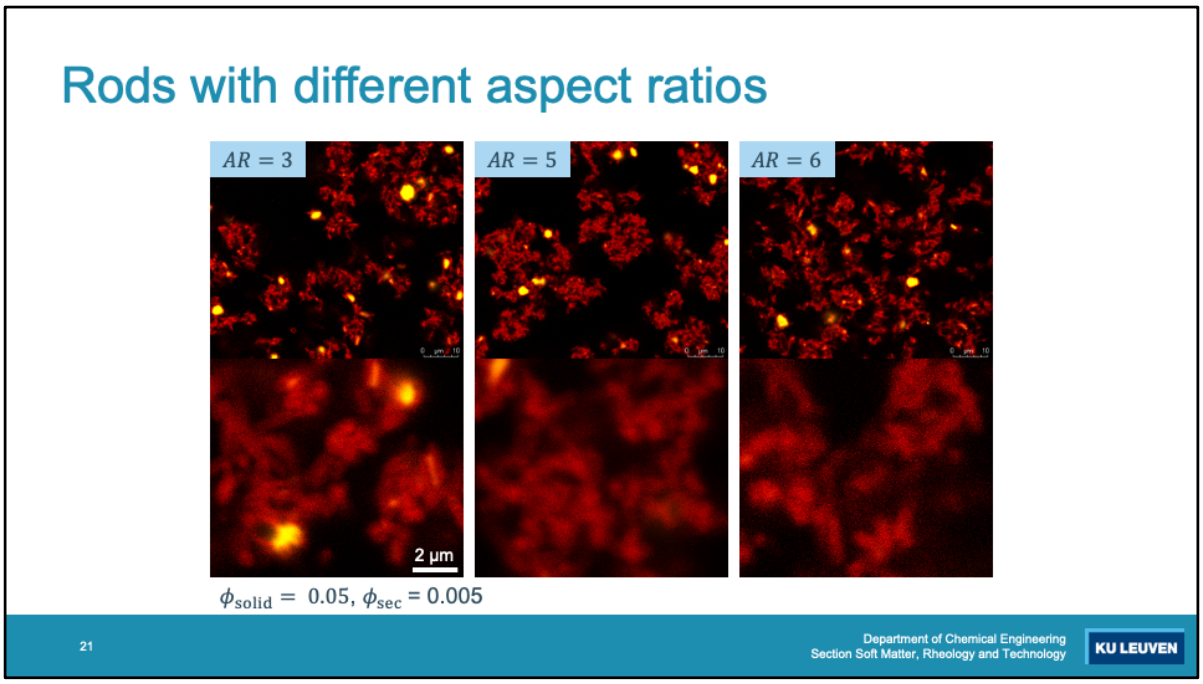

With the help of an exchange student from Delaware finishing her Master thesis in Leuven, we have also had the chance to start investigating the structures formed by rods with different aspect ratios. Here, we can see three examples of networks made with the same solid and secondary fluid fractions. At first glance, you can see the clusters with the lower aspect ratio form denser clusters than the higher aspect ratio. This result is consistent with experiments with particles with other attractive interactions where rods tend to percolate at lower volume fractions than spheres and pack into less dense clusters.

Although these experiments point to an interesting phenomenon, we haven't had the chance to finish due to the shutdown of the labs. Once we get a chance to continue, we will probably opt for slightly larger rods since these particles are too small to detect properly and any, slight mismatch in the index of refraction causes diffraction making such detection even more difficult. While we certainly anticipated this might be a problem, the synthesis route was easier.

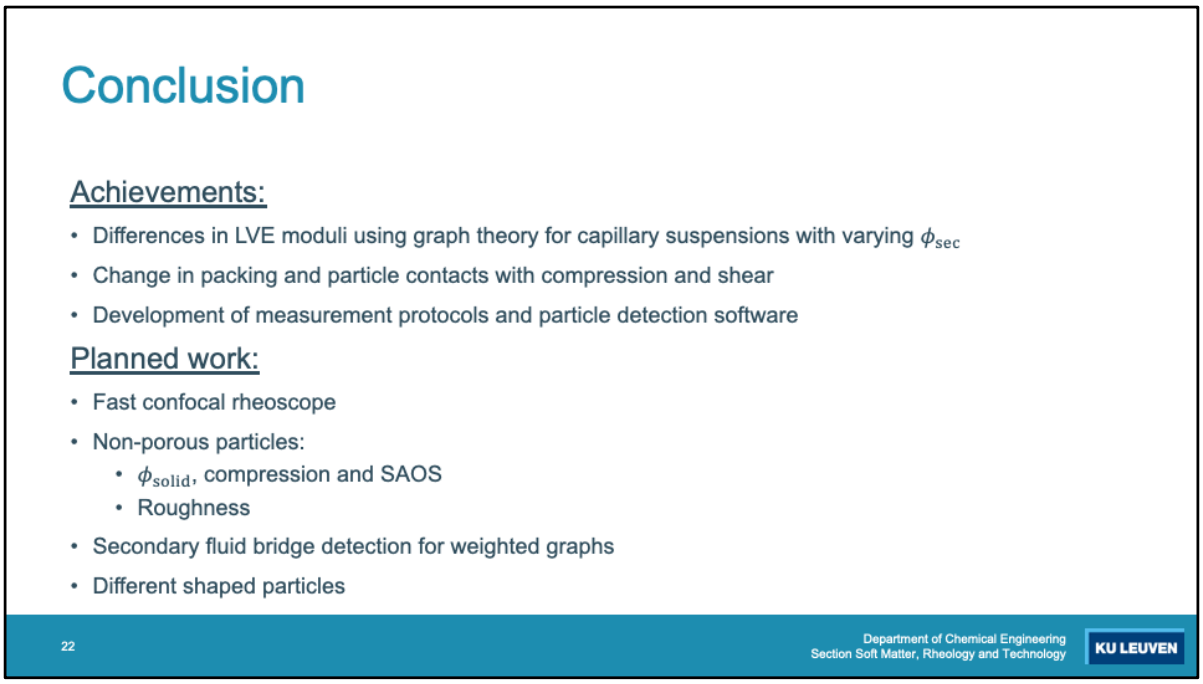

This year we were able to finish the analysis of previous experiments, which showed how measures from graph theory can be used to quantify the transitions that occur with increasing amounts of secondary fluid and can be used to predict the rheological properties of these materials in the linear viscoelastic region. We also conducted initial experiments on samples with different volume fractions, denoting a change from capillary-like behavior at low ϕ_{solid} to granular-like behavior at high loading.

We also used the shutdown period to further improve the measurement protocols and particle detection software. We now have much more accurate detection of the particles with fewer misdetections. These misdetections, caused by intensity differences within the larger particles, will be further improved in the next year when we switch to non-porous particles.

We also observed a curious behavior this year where the roughness of the behavior influenced the bridge type that could be formed. A master student will more rigorously investigate this influence next year. We will also use the non-porous particles to repeat the experiments at different solid fractions and, by including the detection of the secondary fluid bridges to create weighted graphs, we should hopefully link this to the forces between particles and clusters.

Finally, using a fast confocal rheoscope, we can get more information about the dynamic changes in these networks during the shear, more closely linking the stress measurements with the structure.

With that, we want to thank you for listening to (or reading) this presentation. If you have any questions, please feel free to contact me at erin.koos@kuleuven.be

Finally, we would like to welcome you – in better times – to come visit us in Leuven. We are happy to host the ECIS general meeting next year and promise that Willie will not want for good beer.